AGU PUBLICATIONS

Geochemistry, Geophysics, Geosystems

RESEARCH ARTICLE
10.1002/2016GC006498

# Fault zone controlled seafloor methane seepage in the rupture area of the 2010 Maule earthquake, Central Chile

**Jacob Geersen[1], Florian Scholz[1], Peter Linke[1], Mark Schmidt[1], Dietrich Lange[1], Jan H. Behrmann[1], David Völker[2], and Christian Hensen[1]**

[1]GEOMAR Helmholtz Centre for Ocean Research Kiel, Kiel, Germany, [2]MARUM, Center for Marine Environmental Sciences, University of Bremen, Bremen, Germany

**Key Points:**
- We present manifold evidence for active seafloor methane seepage in the rupture area of the 2010 Maule earthquake, Central Chile
- Methane seepage is spatially governed by large upper plate faults that crop out at the upper continental slope
- Recurring plate-boundary earthquakes enhance fault zone permeability, and thus seafloor seepage, over multiple seismic cycles

**Supporting Information:**
- Movie S1
- Table S1
- Table S2
- Table S3

**Correspondence to:**
J. Geersen,
jgeersen@geomar.de

**Citation:**
Geersen, J., F. Scholz, P. Linke, M. Schmidt, D. Lange, J. H. Behrmann, D. Völker, and C. Hensen (2016), Fault zone controlled seafloor methane seepage in the rupture area of the 2010 Maule earthquake, Central Chile, *Geochem. Geophys. Geosyst.*, *17*, doi:10.1002/2016GC006498.

Received 22 JUN 2016
Accepted 3 NOV 2016
Accepted article online 14 NOV 2016



**Abstract** Seafloor seepage of hydrocarbon-bearing fluids has been identified in a number of marine fore arcs. However, temporal variations in seep activity and the structural and tectonic parameters that control the seepage often remain poorly constrained. Subduction zone earthquakes, for example, are often discussed to trigger seafloor seepage but causal links that go beyond theoretical considerations have not yet been fully established. This is mainly due to the inaccessibility of offshore epicentral areas, the infrequent occurrence of large earthquakes, and challenges associated with offshore monitoring of seepage over large areas and sufficient time periods. Here we report visual, geochemical, geophysical, and modeling results and observations from the Concepción Methane Seep Area (offshore Central Chile) located in the rupture area of the 2010 Mw. 8.8 Maule earthquake. High methane concentrations in the oceanic water column and a shallow subbottom depth of sulfate penetration indicate active methane seepage. The stable carbon isotope signature of the methane and hydrocarbon composition of the released gas indicate a mixture of shallow-sourced biogenic gas and a deeper sourced thermogenic component. Pristine fissures and fractures observed at the seafloor together with seismically imaged large faults in the marine fore arc may represent effective pathways for methane migration. Upper plate fault activity with hydraulic fracturing and dilation is in line with increased normal Coulomb stress during large plate-boundary earthquakes, as exemplarily modeled for the 2010 earthquake. On a global perspective our results point out the possible role of recurring large subduction zone earthquakes in driving hydrocarbon seepage from marine fore arcs over long timescales.

## 1. Introduction

The Central Chilean continental margin is known for widespread marine gas hydrates and gas-bearing sediments [e.g., *Bangs et al*., 1993; *Grevemeyer et al*., 2006] and for some locations, methane seeps at the seafloor have been reported [*Sellanes et al*., 2004; *Coffin et al*., 2007; *Jessen et al*., 2011; *Scholz et al*., 2013]. The best studied seep area is the Concepción Methane Seep Area (CMSA in the following) at about 36°S (Figure 1) where methane seepage has been proposed based on dredged fragments of chemosymbiotic clams and carbonate blocks [*Sellanes et al*., 2004], sediment pore water data [*Scholz et al*., 2013], and acoustic and visual observation of seep communities [*Klaucke et al*., 2012; *Zapata-Hernández et al*., 2014]. On 27 February 2010 the CMSA was part of the margin segment affected by the Mw 8.8 Maule earthquake that ruptured a ~500 km long stretch of the plate-boundary offshore Central Chile [e.g., *Vigny et al*., 2011; *Moreno et al*., 2012] (Figure 1A). The Maule earthquake initiated at ~36.5°S and ruptured bilaterally with peak slip of ~15 m in the north [e.g., *Vigny et al*., 2011]. The CMSA, which experienced moderate coseismic slip (~6–9 m), is located between two large slip patches (Figure 1A).

Pore-fluid pressure affects the strength of faults considerably [e.g., *Hubbert and Rubey*, 1959]. This applies to the plate-boundary thrust as well as to faults within the fore arc [e.g., *Saffer and Tobin*, 2011]. Elevated fluid pressure lowers the effective stress along a fault, thus reducing its strength. For many convergent margins such as Nankai, Barbados, and Central America, a lack of seismicity at the shallow region of the plate-boundary fault has been related to fluids that weaken the fault zone [*Moore et al*., 1998; *Tobin et al*., 2001; *Screaton et al*., 2002; *Ranero et al*., 2008; *Bangs et al*., 1999, 2004, 2015]. In contrast, deeper regions of the plate-interface that tend to rupture during large earthquakes usually are made up of rocks having

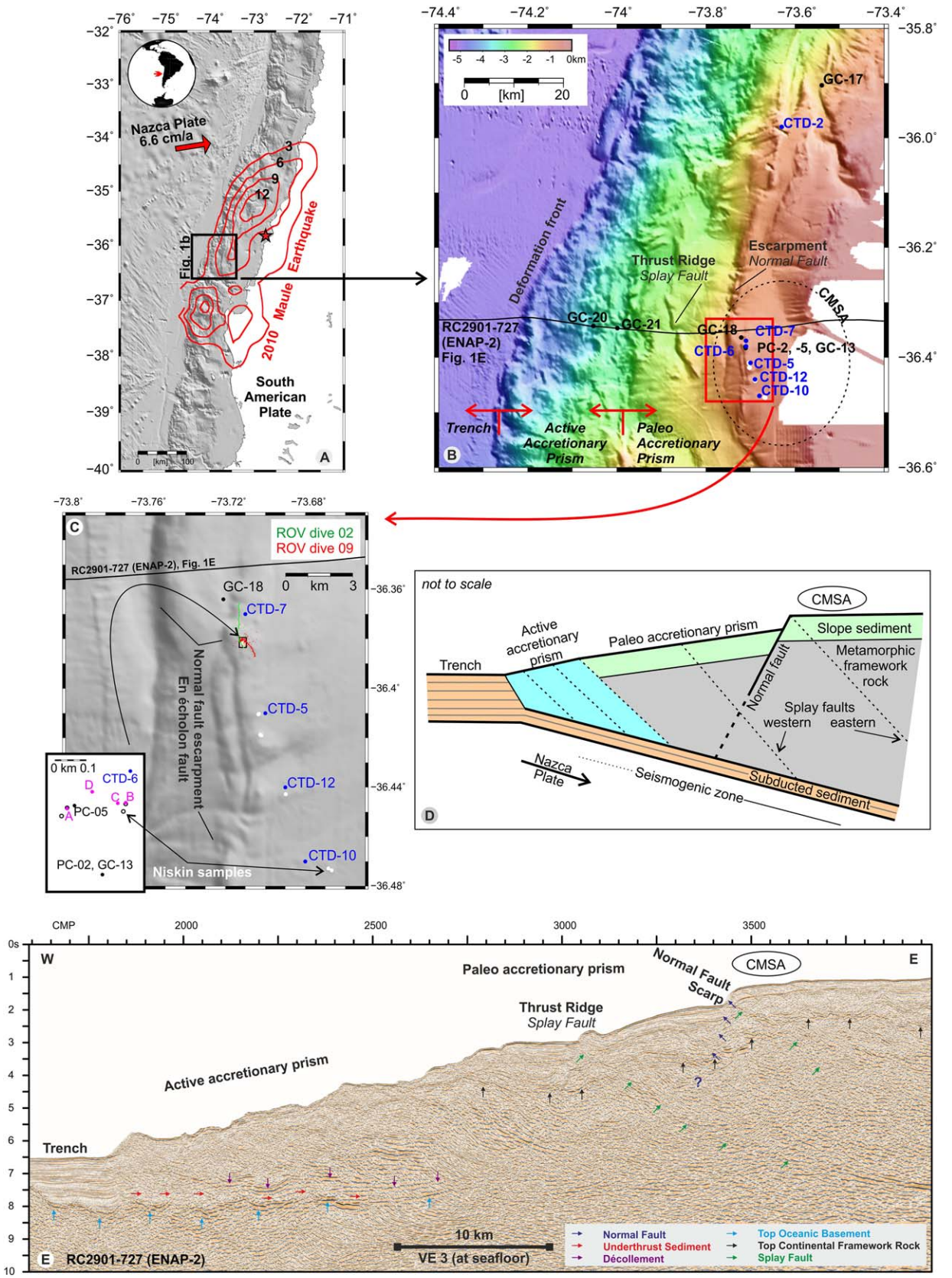


Geersen - G-cubed - Figure 1

considerable cohesion and potentially high friction [e.g., *Ikari et al*., 2011; *Schumann et al*., 2014]. However, by providing potential pathways for fluid-migration, fore-arc faults themselves affect fluid pressure and thus the degree of coupling along the underlying plate-boundary [*Saffer and Tobin*, 2011]. The interplay of faulting and fluid flow is further complicated by the different stress states that a fore arc undergoes during a seismic cycle. The normal mode of horizontal compression that dominates in most of the marine fore arc during the interseismic period tends to obstruct fluid flow along faults. In contrast, the same fault zones may become conduits for fluids during the short coseismic and postseismic phase of horizontal extension [*Husen and Kissling*, 2001; *Grevemeyer et al*., 2006]. Good knowledge on the relation of faulting and fluid flow is crucial to better understand the structural and tectonic controls on fluid seepage in marine fore arcs.

To better understand fluid flow and seafloor seepage in a seismically active area, R/V SONNE (cruise SO210) visited parts of the rupture area of the 2010 Maule earthquake, including the CMSA, 7 month after the main shock [*Linke*, 2011]. In this work we link visual seafloor observations (remotely operated vehicle (ROV) surveys), geochemical measurements in the water column and the shallow sediments (methane, sulfate, ethane, and propane), geophysical data, and stress modeling results. We do this in order to provide a comprehensive evaluation of seafloor methane seepage in the CMSA as well as to investigate the structural and tectonic controlling parameters.

### 1.1. Tectonic Setting of the Central Chilean Marine Fore Arc

The Chilean continental margin in the area of the 2010 Maule earthquake is shaped by the subduction of the Eocene-Oligocene oceanic Nazca Plate under the South American Plate (Figure 1A) [e.g., *Tebbens and Cande*, 1997]. With ~2–3 km of trench sediment at the deformation front [*Völker et al*., 2013], the investigated segment of the margin is currently in an accretionary phase, which started in middle Miocene or Pliocene [*Behrmann et al*., 1992; *Kukowski and Oncken*, 2006; *Melnick and Echtler*, 2006]. The current phase of accretion was preceded by subduction erosion or nonaccretion in the Paleogene that must have removed parts of a Paleogene-Mesozoic paleoaccretionary prism [*Kukowski and Oncken*, 2006]. Perpendicular to the trench, the marine fore arc is divided into the currently active accretionary prism between the deformation front and ~2000 m water depth and the paleo-accretionary prism upslope of the active accretionary prism (Figures 1B, 1D, and 1E) [*Bangs and Cande*, 1997; *Contreras-Reyes et al*., 2010; *Geersen et al*., 2011]. In the paleo-prism a bright high-amplitude reflector in seismic reflection data represents the top of the metamorphic framework rock that is buried under ~1–2 km of slope sediment (Figures 1D and 1E) [see also *Bangs and Cande*, 1997; *Geersen et al*., 2011].

At around 1000 m water depth, the seafloor is offset by a large (800 m seafloor offset) seaward dipping normal fault (Figures 1B–1E) [*Geersen et al*., 2011]. Around 36.4°S, at the latitudes where the CMSA is located, the normal fault scarp is offset toward the continent by about 3 km (Figures 1B and 1C). The offset points toward the possible presence of an en échelon fault, which likely soles into the same master fault at depth. Seismic reflection data do not resolve the deep continuation of the normal fault, or a possible intersection with the plate-boundary fault or its splays, but show that the normal fault penetrates into the framework rock of the paleo-prism (Figure 1E). Growth strata in the hanging wall of the normal fault indicate that it is active [cf. *Geersen et al*., 2011, Figure 3e]. In addition to the normal fault, the paleo-prism in the area of this study hosts two splay faults, from which the eastern one (the one located closer to the coast), crops out at the seafloor in the CMSA (Figures 1B, 1D, and 1E) [*Geersen et al*., 2011].

**Figure 1.** (A) Overview map of the Central Chilean continental margin. The epicenter of the 27 February 2010 Mw. 8.8 Maule earthquake is indicated by the red star. Slip contour lines are given in meters [*Vigny et al*., 2011]. (B) Bathymetric map of the study area with the approximate location of the Concepción Methane Seep Area (CMSA) outlined by the black dashed ellipse. The main structural elements perpendicular to the slope are the trench, the active accretionary prism, and the paleo-accretionary prism (compare Figures 1D and 1E). A prominent seaward dipping escarpment (up to 800 m seafloor offset) that can be traced over about 50 km along the upper continental slope indicates the seafloor outcrop of a large normal fault. The red box in the footwall of the normal faults indicates the area where the seafloor fractures where documented during ROV dives 2 and 8 (compare Figure 1C). Black dots indicate locations of gravity cores (GC) and push cores (PC). Blue dots show CTD locations and white dots highlight locations where water samples have been taken with the ROV (Niskin bottles) directly above the seafloor. (C) Shaded relief map showing the tracks of ROV dives 2 (green dots) and 8 (red dots). The exact locations of the seafloor fractures (purple dots) is shown in the small inset in the bottom left corner. Black circles indicate locations of gravity cores (GC) and push cores (PC), blues circles are CTD locations and white circles are water samples taken during ROV dives (Niskin bottles) directly above the seafloor. (D) 2-D sketch across the continental margin showing the main structural and tectonic elements of the study area (not to scale). (E) Seismic reflection line RC2901-727 (ENAP-2) across the study area (compare Figures 1B and 1C for location) highlighting the main structural and tectonic elements of the marine fore arc discussed in this study [cf. *Bangs and Cande*, 1997; *Geersen et al*., 2011].

## 2. Data and Results

### 2.1. ROV-Video Observations From the CMSA

The ROV (remotely operated vehicle) KIEL 6000 is a 6000 m rated electric work class ROV manufactured by Schilling Robotics LLC (www.geomar.de/en/centre/central-facilities/tlz/rovkiel6000). Tools standardly installed on the vehicle include a HDTV camera, two high-resolution color zoom cameras, and one digital still camera as well as three black and white observation cameras. Besides the video capabilities, the two manipulator arms are the major tools used on the platform. Further tools include a DIGIQUARTZ depth sensor, a SBE49 FastCAT CTD, a SIMRAD sonar system, a PNI TCM2-50 compass, a motion reference unit (MRU) containing a gyro compass, and an RDI Doppler velocity log. For navigation, the USBL-based IXSEA POSIDONIA$^{TM}$ system was employed. The tool sled in the lowermost part of the vehicle is dedicated to take up the scientific payload. During cruise SO210, the port side sample tray was rigged for sampling push cores. On the front plate of the drawer, two 5 L Niskin bottles for water samples were mounted.

Two ROV dives conducted in the CMSA in the footwall of the large normal fault (compare Figure 1C for location) revealed a series of elongated fractures with diameters in the range of 0.05–0.5 m and along-slope lengths between 0.5 and 5 m (Figure 2, also see videos in Supporting Information). The fractures occur about 100 m landward of the scarp that likely represents an en écholon structure merging into the large normal fault at depth (compare inset in Figure 1C for exact location of fractures). They trend N-S to NW-SE and are, thus, subparallel to the large normal fault scarp. At one location a prominent ~N-S striking escarpment that may represent the top of the normal fault scarp was documented, with a parallel striking fracture located directly behind (fracture D; Figure 2). All fractures show little to no signs for degradation with sharp edges and partly overhanging cliffs. Unfortunately, the total area covered by the ROV video observations is limited to less than $<0.5$ km$^2$. However, the fact that we found multiple fractures within this limited area

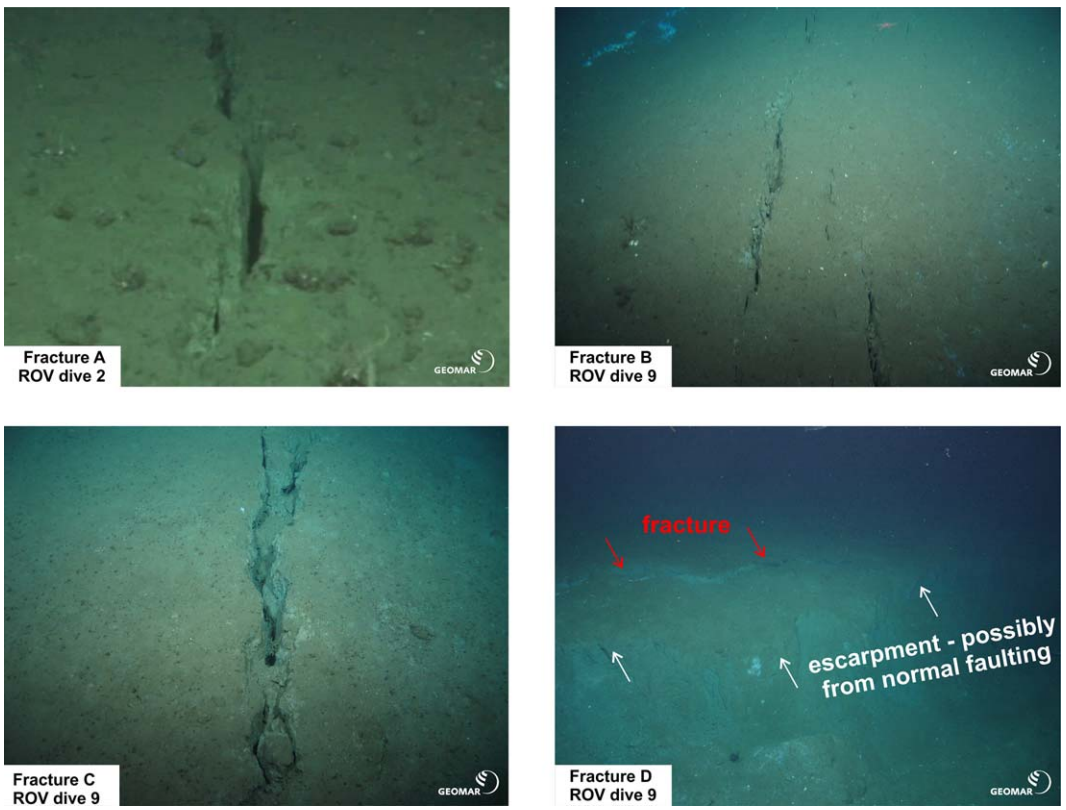


**Figure 2.** Seafloor fractures documented during ROV dives in the footwall of the large normal fault (compare the inset in the bottom left corner of Figure 1C for the exact locations of the fractures). All fractures trend N-S to NW-SE with diameters in the range of 0.05–0.5 m and along-slope lengths between 0.5 and 5 m. In case of fracture D a prominent escarpment that may represent the normal fault scarp, is visible just westward (seaward) of the fracture.

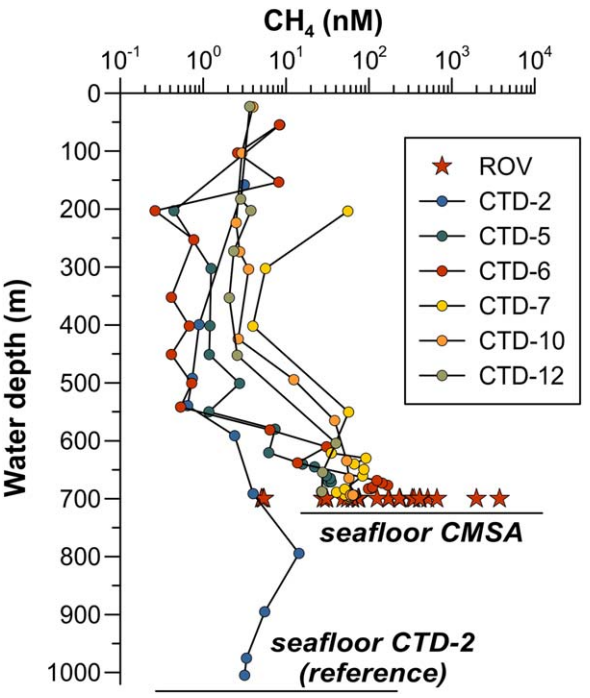


**Figure 3.** Methane concentrations in the water column from the Concepción Methane Seep Area (CMSA) and a reference site (CTD-2) about 50 km farther north (compare Figures 1B and 1C for sample locations). Circles indicate water samples obtained with the CTD and stars indicate samples obtained with the ROV (Niskin bottles) directly above the seafloor. Upper black horizontal line indicates the average depth of the seafloor in the CMSA and lower black horizontal line indicates the depth of the seafloor at the location of CTD-2.

suggests that similar features are possibly located elsewhere in the CMSA in the area of the large normal fault.

### 2.2. Methane Concentrations in the Water Column

Water column measurements were mainly carried out with the onboard Conductivity-Temperature-Depth (CTD) system. The CTD system consisted of a carousel with a SBE9-plus CTD (Sea-Bird Electronics, Inc., Washington, USA) equipped with standard sensors (Conductivity, Temperature, Pressure, and Dissolved Oxygen), a pH sensor, and a 24 Niskin bottle rosette for discrete water sampling. At each CTD station water samples were collected at different water depths. In addition to water sampling during CTD casts, additional water samples were taken about 1 m above the seafloor with Niskin bottles during ROV dives. After onboard recovery, all water samplers were immediately subsampled into preevacuated glass bottles following the degassing method described in *Keir et al*. [2008]. The gas released by the vacuum degassing technique was stored in septum-stoppered glass vials for subsequent onboard concentration measurements. Methane concentrations were determined by using a "Thermo Trace ultra" gas chromatograph with a precision of ±3% (RT Alumina bond-KCL capillary column; He carrier gas, FID detector).

To determine water column methane concentration in the CMSA, we conducted five CTD casts along a 10 km long transect with CTD-6 located in direct vicinity (∼100 m) of the juvenile fractures (Figures 1B and 1C). The CTD data were complemented with water samples from about 1 m above the seafloor that were taken during ROV dives by means of Niskin bottles (white dots in Figures 1B and 1C). For comparison we also conducted a CTD cast ∼50 km farther north, outside of the outcrop area of the large normal fault (CTD-2, Figure 1B). Far above the seafloor (0–450 m water depth), water column methane concentrations in the CMSA usually range between 0.1 and 10 nM (Figure 3). However, during the two CTD casts located closest to the fractures, concentrations of up to 8 nM (CTD-6, at 55 m water depth) and 56 nM (CTD-7, at 203 m water depth) are also observed. Below ∼450 m water depth (CTDs-7, −10, −12) or ∼550 m water depth (CTDs-5, −6) methane concentrations increase everywhere in the CMSA to values up to 169 nM (CTD-6) and 3776 nM (Niskin bottle) close to the seafloor. Outside of the CMSA at CTD site 2 a maximum methane concentration of 15 nM is observed at about 800 m water depth and the concentrations decrease toward the seafloor (Figure 3).

### 2.3. Sediment Sampling for Pore Water Sulfate and Hydrocarbon Data

Sediment samples were obtained by the aid of a gravity corer and ROV-guided push cores. Upon recovery, gravity cores (GC) were cut into 1 m sections and split into halves. One half was used for visual inspection and description, the other half was used for sediment subsampling and pore water recovery. Push cores (PC) were stepwise extruded from the core liner and sectioned in 1–4 cm thick discs. The pore water was recovered using a sediment squeezer at pressures between 3 and 5 bar. After squeezing, pore waters were filtered through cellulose acetate membrane filters. Sulfate ($SO_4^{2-}$) concentrations were determined by ion chromatography. For pore water hydrocarbon analysis, 3 mL of undisturbed sediment were disaggregated

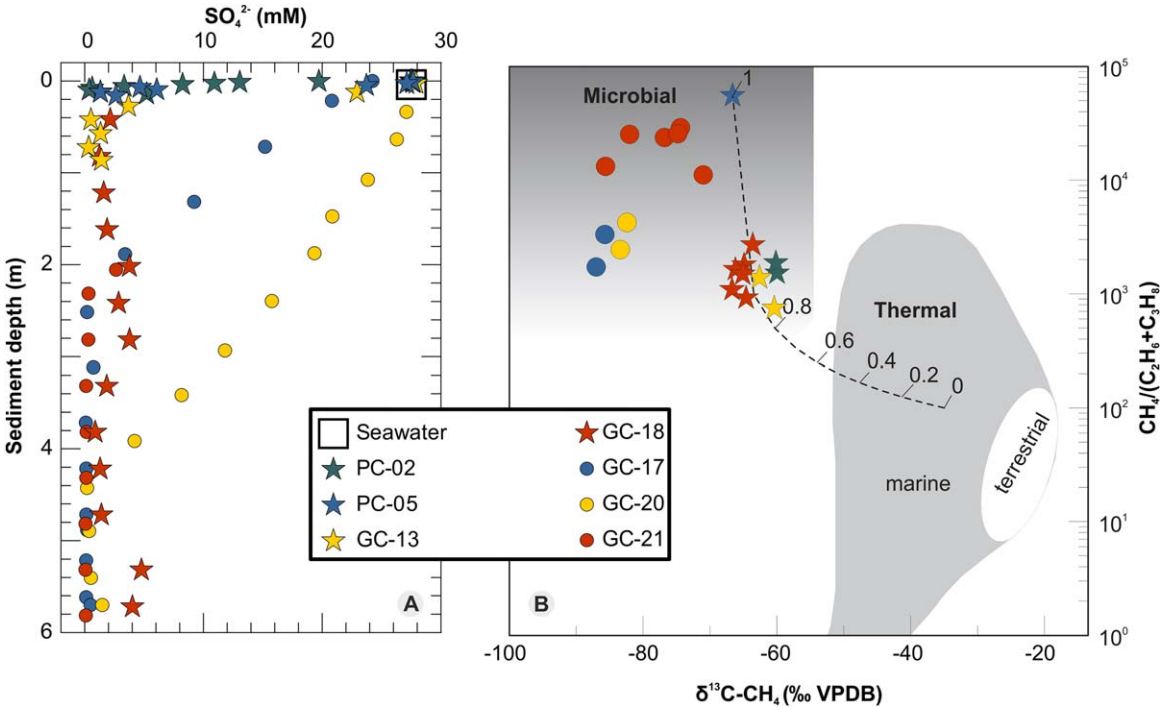


**Figure 4.** (A) Pore water sulfate concentrations from sediment samples obtained by gravity cores (GC) and push cores (PC). Stars represent samples from within the CMSA and circles represent samples from farther north or downslope (compare Figures 1B and 1C for sample locations). The depth of sulfate penetration ranges from ~0.1 to 0.4 m in cores from within the CMSA to ~2–5 m in cores from further downslope (also compare Table 1). (B) Stable carbon isotope composition of sedimentary methane plotted against the ratio of methane over ethane and propane in a modified Bernard diagram (according to *Faber et al.* [2015]). To exclude fractionation effects associated with microbial hydrocarbon oxidation within the sediments, only samples from below the sulfate penetration depth are considered. A two-end-member mixing line calculated with a microbial end-member (PC05) and a postulated thermogenic end-member is shown as a dashed line (plotted numbers indicate the fraction of microbial methane, 1 = 100%).

and dispersed in 20 mL sealed glass vials, immediately after core retrieval. The glass vials also prefilled with 9 mL 1.0 M sodium hydroxide were stored and shipped at 4°C for subsequent laboratory analyses at GEOMAR. The hydrocarbon concentrations in the head space of the vials were analyzed by gas chromatography (Thermo Trace Ultra, FID detector, capillary column RT-Alumina bond-KCl). Stable carbon isotope ratios of methane (reported in delta notation ‰ relative to Vienna Pee Dee Belemnite, VPDB) were determined by "continuous flow GC-combustion isotope ratio mass spectrometry" (Thermo Trace GC coupled to Thermo MAT253) with a reproducibility of ±0.3 ‰ (2 standard deviations). Sedimentary total organic carbon (TOC) concentrations were determined with a Carlo Erba Element Analyzer after separation of inorganic carbon through treatment with 1.0 M hydrochloric acid. Detailed information about the methods applied during and after the SO210 cruise are given in *Scholz et al.* [2013] and http://www.geomar.de/en/research/fb2/fb2-mg/benthic-biogeochemistry/mg-analytik/.

We present pore water sulfate and hydrocarbon data for two PCs (PC-02 and PC-05) and two GCs (GC-13 and GC-18) from within the CMSA as well as three GCs (GC-17, GC-20, and GC-21) from farther north or downslope (Figure 4A and Table 1). Pore water data of GC-17–GC-21 were previously published by *Scholz et al.* [2013]. All pore water sulfate profiles show a downward decrease from bottom water values around 28 mM close to the seafloor to values near zero at greater depth. The sulfate penetration depth ranges from ~0.1–0.4 m in cores from within the CMSA to ~2–5 m in cores from further downslope. The carbon isotope composition of dissolved methane is plotted against the ratio of methane

**Table 1.** Depth of Sulfate Penetration (Compare Figure 3) and Mean TOC Concentrations for Cores Discussed in This Study [cf. *Scholz et al.*, 2013]

| Core | Sulfate Penetration Depth (cm) | Mean TOC (wt %) | Standard Deviation |
|---|---|---|---|
| PC02 | 8 | 0.93 | 0.10 |
| PC05 | 13 | 1.08 | 0.15 |
| GC13 | 43 | 0.66 | 0.29 |
| GC18 | 42 | 0.84 | 0.28 |
| GC17 | 444 | 1.30 | 0.74 |
| GC20 | 443 | 1.07 | 0.27 |
| GC21 | 232 | 2.69 | 0.25 |

over ethane and propane in Figure 4B ("Bernard Diagram" after *Bernard et al*. [1978] and *Faber and Stahl* [1984]). To exclude fractionation effects associated with hydrocarbon oxidation, only samples from below the sulfate penetration depth are considered in Figure 4B. All data plot within the field defined by microbial methane formation, however, CMSA data ($\delta^{13}C_{CH4} = -60$ to $-66‰$; star symbols in Figure 4B) are slightly shifted toward a thermogenic origin when compared to samples from outside the CMSA ($\delta^{13}C_{CH4} = -70$ to $-86‰$; circles in Figure 4B). Neither sulfate penetration depth nor $\delta^{13}C_{CH4}$ data show a significant correlation with the TOC content of the cores (Table 1).

### 2.4. Coulomb Stress Induced Into the Upper Plate by the 2010 Maule Earthquake

During a large plate-boundary earthquake, the part of the marine fore arc landward of the maximum rupture area, experiences a reversal in the stress state from predominantly horizontal compression to predominantly horizontal extension [*Klotz et al*., 1999; *Hardebeck*, 2012]. To investigate if the extensional stress induced into the upper plate by the 2010 Maule earthquake was sufficient to trigger normal faulting and to support hydraulic fracturing and fault dilation in the area of the CMSA, we compute the coseismic Coulomb stress change [e.g., *King et al*., 1994]. Our calculations are made in an elastic half-space with uniform isotropic elastic properties following *Okada* [1992] and the coseismic rupture model of *Vigny et al*. [2011]. We investigate the stress change for optimal oriented normal faults at 10 km depth with the optimal orientation defined by the maximum value of Coulomb stress change modeled at each grid.

Coulomb stress change computations show that the 2010 Maule earthquake induced an extensional stress regime in the marine fore arc at 10 km depth in the area of the CMSA (Figure 5). *Aron et al*. [2013] investigate the Coulomb stress change for the Maule rupture using a variety of different coseismic slip models. Consistent with our modeling results, they postulate that the Maule earthquake induced an extensional Coulomb stress increase in the marine fore arc at distances larger than ~20 km landward from the trench.

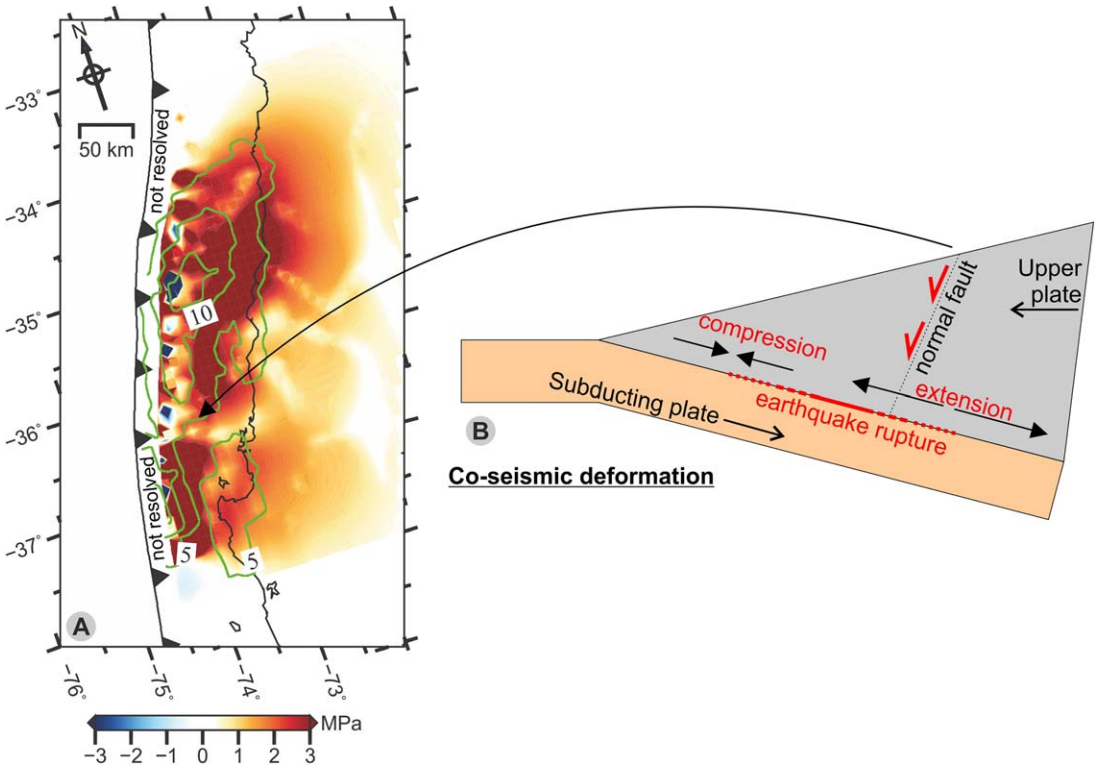


**Figure 5.** (A) Coulomb stress change induced by coseismic rupture of the 27 February 2010 Mw. 8.8 Maule earthquake (slip model from *Vigny et al*. [2011]) calculated for optimally oriented normal faults at 10 km depth. The fore arc in the study area shows positive values of Coulomb stress change thus favoring normal faulting oriented subparallel to the plate boundary (see *Aron et al*. [2013] for an in-depth discussion). Marine fore arc compression in the area of the lowermost slope, as indicated in the conceptual drawing, is not resolved in the model due to the intersection of the plane at 10 km with the subducting slab. Green lines indicate coseismic slip contour lines (5 m intervals). (B) Conceptual drawings illustrating the stress change in the marine fore arc during the coseismic phase.

## 3. Discussion

### 3.1. Activity of Seafloor Methane Seepage in the CMSA

The water column overlying the CMSA shows a significant positive methane anomaly (factor 10–1000 above background) indicating active methane release from the seafloor (Figure 3). With 8 nM at 55 m water depth (CTD-6) and 56 nM at 203 m water depth (CTD-7) it seems plausible that some of the methane in the CMSA even reaches the atmosphere. For the shallow water we can, however, not ultimately distinguish if the high methane concentrations result from a plume that rises from the seafloor or if they originate from a different water mass enriched in methane. In addition to the methane anomalies in the water column, the sulfate penetration depth in surface sediment, which is controlled by microbial sulfate reduction coupled to anaerobic methane oxidation [*Niewöhner et al*., 1998; *Hensen et al*., 2003], can be used as a proxy for the methane flux from subsurface sediment strata [*Borowski et al*., 1996]. The comparably shallow sulfate penetration depth in the CMSA (<0.4 m), compared to the cores from farther north and downslope (2–5 m) further indicates a higher seafloor methane flux (Figure 4A and Table 1).

From the methane and the sulfate data we classify the seepage activity in the CMSA in fall 2010 as high. Methane concentrations of up to 3776 nM directly above the seafloor and the observed spatial variations over 3 orders of magnitude are for example comparable to other prominent active margins seep systems such as Hydrate Ridge off Cascadia margin [e.g., *Heeschen et al*., 2005]. However, in contrast to other active seep areas, which have been visited by multiple measurement campaigns, we are lacking data to quantify temporal changes in seep activity. The only other direct measurement of seep activity from the CMSA are side-scan sonar data collected in 2008 [*Klaucke et al*., 2012], 2 years before the 2010 Maule earthquake. Based on their data, *Klaucke et al*. [2012] report an obvious enigma between widespread evidence for fossil cold seeps in the form of high backscatter anomalies on the seafloor that reflect authigenic carbonate precipitates, and little evidence for active seepage. Within their ~800 $km^2$ of side-scan data they found only a couple of gas flares in the water column. Nevertheless, the different techniques used in 2008 (side-scan sonar) and 2010 (water column and sediment sampling) do not allow to draw a final conclusion if seepage has increased within the 2 years.

### 3.2. Origin of the Methane

To investigate the origin of the methane that is released in the CMSA, we measured its stable carbon isotope signature ($\delta^{13}C\text{-}CH_4$) (Figure 4B). The methane could be exclusively produced at shallow depth (tens of meters) and transported into the SMTZ by diffusion or it could be derived from greater depth (hundreds to thousands of meters) and transported into the shallow sediments through advective transport along faults or other weak zones [*Schmidt et al*., 2005]. If shallow microbial methane production was the exclusive reason for the high methane flux in the CMSA, one would expect sulfate penetration to correlate with the current rate of organic matter delivery which can be roughly estimated from TOC concentrations (Table 1). We do not observe such a correlation. In fact, TOC concentrations in slope basins further downslope are substantially higher than in the CMSA, despite a greater sulfate penetration depth (Table 1) [cf. *Scholz et al*., 2013]. This observation suggests that at least some of the methane released in the CMSA must derive from deeper strata.

An admixture of methane from greater depth in the CMSA is further consistent with previously published calculations of the stoichiometry of sedimentary sulfate consumption to bicarbonate production across the Chilean margin [*Scholz et al*., 2013]. Moreover, the elevated $\delta^{13}C_{CH4}$ values in sediments of the CMSA (stars in Figure 4B) are indicative for a higher proportion of thermogenic hydrocarbon gas compared to cores from outside the CMSA (circles in Figure 4B). Thermogenic hydrocarbon gas production requires temperatures beyond the 5–60°C [*Claypool and Kvenholden*, 1983] that prevail within the hemipelagic sediments overlying the paleo-accretionary prism [*Scholz et al*., 2013]. We therefore assume that the methane released in the CMSA is a mixture of shallow biogenic methane with thermogenic methane that is derived from deeper strata. A mixing line calculated by using a microbial hydrocarbon end-member (PC05 in Figure 4B and Table 1) and a thermogenic end-member ($\delta^{13}C_{CH4} \sim -35‰$, $C1/(C2+C3) \sim 100$) joins all the CMSA data in the modified Bernard plot (Figure 4B) [*Faber et al*., 2015]. The rough calculation may indicate possible admixing of up to 20% of mature thermogenic methane to shallow microbial methane within the CMSA (i.e., "0.8" in Figure 4B). A possible thermogenic methane source at greater depth could either be organic-

rich compacted framework rock of the paleo-accretionary prism or subducted sediments along the plate boundary, or a combination of both.

### 3.3. Possible Links Between Seafloor Methane Seepage and the Seismic Cycle

Coulomb stress change calculations (Figure 5) suggest that the transfer of stress into the upper plate caused by the coseismic rupture of the 27 February 2010 Mw. 8.8 Maule earthquake could have caused extensional faulting in the marine fore arc in the area of the CMSA. In fact, extensional rupture in the upper plate in the wake of a large plate-boundary earthquake has been documented in the northern termination of the rupture area of the 2010 Maule earthquake [e.g., *Farias et al*., 2011; *Lange et al*., 2012] as well as after the giant 2011 Mw 9.0 Tohoku-Oki earthquake [*Tsuji et al*., 2013]. In the case of the 2011 Tohoku-Oki earthquake comparable open fissures and fractures were visually documented at the seafloor overlying seismically imaged upper plate normal faults [*Tsuji et al*., 2013]. There, repeated video observations conducted between 2002 and 2012 showed that the fractures were not present in the years before the earthquake suggesting that they formed due to coseismic rupture during the 2011 Tohoku-Oki earthquake.

The location of the large normal fault in the CMSA and its strike direction parallel to the trench (Figure 1B) makes this structure an ideal candidate for the release of some of the stresses transmitted into the upper plate prior to large plate-boundary earthquakes, and released during the earthquakes. The uneroded edges of the fractures and lack of sedimentary infill (Figure 2) suggest that they represent relatively young (days to couple of years) extensional features, possible related to extensional rupture across the underlying large normal fault during or shortly after the 2010 Maule earthquake. We therefore expect similar seafloor fractures elsewhere in the CMSA. However, we are not able to proof this with the limited spatial coverage ($<$0.5 km$^2$) of the ROV video observations.

In addition to normal faulting, the extensional stresses that prevail in the upper plate in the area of the CMSA during large plate-boundary earthquakes (including during the 2010 Maule earthquake) may support hydraulic fracturing and dilation of existing faults. This results in an increase in permeability along both large upper plate faults that crop out in the CMSA; i.e., the normal fault and the eastern splay-fault. The reopening of faults in an extensional stress regime is one viable mechanism to enhance the permeability of accretionary wedges to considerable depth [*Behrmann*, 1991]. In the case of indurated lithologies (cohesion of 5 MPa), reopening of weakly cemented hydraulic fractures is possible to depths of over 1 km and an even greater depth of reopening is possible in overpressured environments [see *Behrmann*, 1991, Figures 3 and 4].

Based on the spatial correlation between the large upper plate faults (normal fault and eastern splay fault), the juvenile extensional fractures, the high water column methane concentrations, and the shallow sulfate penetration depth, we propose a conceptual model (Figure 6) to link seafloor hydrocarbon seepage in the CMSA to the frequently recurring plate-boundary earthquakes:

1. Large subduction earthquakes induce a regime of extension in the marine fore arc in the area of the CMSA, large enough to reactivate the normal fault and to create extensional fractures at the seafloor.
2. Extension of the upper plate further results in hydraulic fracturing and dilation of the normal-fault and the eastern splay fault that both underlie the CMSA. This together increases the permeability along the faults, allowing them to become hydraulically communicative with the deep fore arc-strata and possibly the plate boundary.
3. As a consequence, fluid pulses from the upper plate and/or the plate boundary move upward along the faults resulting in the observed seepage.

The model can well be transferred to other subduction zone settings such as Makran, where the 1945 Mw. 8.1 earthquake seems to have triggered hydrocarbon seepage from the continental slope [*Fischer et al*., 2013] and where huge upper plate normal faults have been seismically imaged [*Grando and McClay*, 2007]. Furthermore, the model may also explain basic differences in the spatial distribution of seep sites at the accretionary margin of Central Chile, relative to an erosive plate margin as for example Costa Rica. In the latter case, tectonic erosion at the base of the overriding plate causes widespread subsidence and related normal faulting all over the continental slope. As a consequence, fluid seepage distributes over most of the continental slope, locally extending down to the deformation front [*Hensen et al*., 2004; *Ranero et al*., 2008; *Sahling et al*., 2008]. In central Chile, however, viable conditions for extensional tectonics are only met in the coseismic phase. Here fore-arc extension, and therewith also seep activity, is spatially limited to the upper

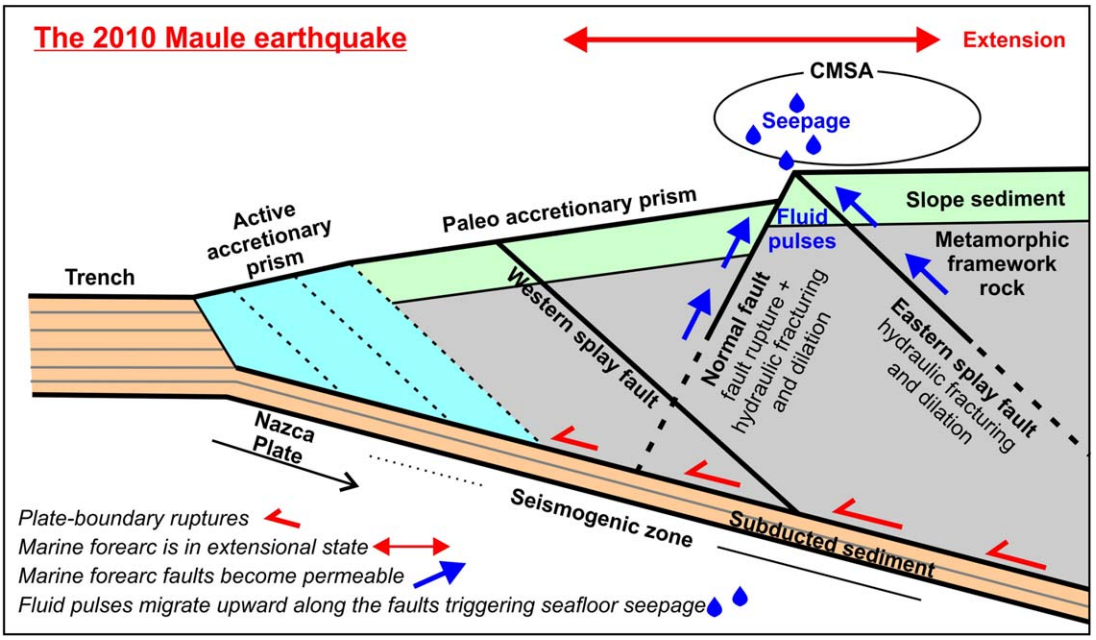


**Figure 6.** Conceptual model illustrating how seismic rupture during the 2010 Maule earthquake governed extensional faulting, fluid flow, and hydrocarbon seepage in the Concepción Methane Seepage Area (CMSA).

continental slope and shelf area landward of the area of peak rupture during large plate-boundary earthquakes (compare Figure 5B).

In the case of a single earthquake one would expect progressive recementation and healing of the faults and the extensional fractures and concurrent cessation of fluid flow after the earthquake. However, the recurrence rate of large plate-boundary earthquakes in the study area is only in the range of 100–150 years [*Lomnitz*, 2004]. Even if not every single earthquake induces extensional stresses large enough to trigger activity of the large upper plate faults, the interseismic period is possibly not long enough to allow for a complete healing of the fluid pathways. It is thus likely that fluid flow along the faults and related seafloor methane seepage continue to some extent over long timescales and do not cease completely during a seismic cycle. This is further supported by the local occurrence of gas flares in the water column in the CMSA, which *Klaucke et al.* [2012] reported from their thorough investigation of side-scan sonar data collected in 2008, about 2 years before the 2010 Maule earthquake. Continuously high seep activity over multiple seismic cycles is further in-line with the widespread evidence for fossil cold seeps in the area reported by *Klaucke et al.* [2012]. However, repeated measurements in between large plate-boundary earthquakes are needed to quantify a possible temporal variability of fault-related methane seepage on the Central Chilean marine fore arc in relation to the seismic cycle.

## 4. Conclusion

We here present evidence for active seafloor methane seepage in the rupture area of the 2010 Mw. 8.8 Maule earthquake about half a year after the earthquake. Coulomb stress calculations and the visual observation of juvenile extensional cracks at the seafloor suggest that the upper plate in the area of the seepage is exposed to an extensional stress regime during large plate-boundary earthquakes; as exemplarily modeled for the 2010 Maule earthquake. The recurring extensional stresses result in activity, hydraulic fracturing, and dilation of large upper plate faults, therewith supporting the upward movement of fluid pulses and the seepage of hydrocarbon bearing fluids from the marine fore arc. Repeated measurement campaigns over multiple years/decades are however needed to quantify changes in seep activity over a complete seismic cycle. In line with recent findings from the Makran margin [*Fischer et al.*, 2013] our results suggest that large subduction zone earthquakes have the potential to alter hydrocarbon export to the ocean and possibly the atmosphere.

**Acknowledgments**
We thank captain and crew of R/V SONNE and the ROV team for professional support during cruise SO210. Bettina Domeyer, Ulrike Lomnitz, Asmus Petersen, Regina Surberg, and Peggy Wefers are acknowledged for assistance during sampling and onboard chemical analyses. We thank Ingo Klaucke for discussion of the side-scan data and Nathan Bangs for his comments on an earlier version of the manuscript. Lori Summa and an anonymous reviewer are thanked for the many constructive comments that helped us to improve the manuscript. R/V SONNE Cruise SO210 was carried out in the framework of the Sonderforschungsbereich (SFB) 574 "Volatiles and fluids in subduction zones" at Kiel University both funded by the DFG. Jacob Geersen was funded by a grant (CP1404) of the Cluster of Excellence 80 "The Future Ocean." The Future Ocean is funded within the framework of the Excellence Initiative by the Deutsche Forschungsgemeinschaft (DFG) on behalf of the German federal and state governments. The 7th Framework Program of the European Union supported the participation of Florian Scholz (Marie Curie IOF #300648, BICYCLE).

## References

Aron, F., R. W. Allmendinger, J. Cembrano, G. González, and G. Yáñez (2013), Permanent fore-arc extension and seismic segmentation: Insights from the 2010 Maule earthquake, Chile, *J. Geophys. Res.*, *118*, 724–739, doi:10.1029/2012JB009339.

Bangs, N. L., and C. S. Cande (1997), Episodic development of a convergent margin inferred from structures and processes along the southern Chilean margin, *Tectonics*, *16*, 489–503.

Bangs, N. L., D. S. Sawyer, and X. Golovchenko (1993), Free gas at the base of the gas hydrate zone in the vicinity of the Chile triple junction, *Geology*, *21*, 905–908.

Bangs, N. L., T. H. Shipley, J. C. Moore, and G. F. Moore (1999), Fluid accumulation and channeling along the northern Barbados Ridge décollement thrust, *J. Geophys. Res.*, *104*, 20,399–20,414, doi:10.1029/1999JB900133.

Bangs, N. L., T. Shipley, S. Gulick, G. Moore, S. Kuromoto, and Y. Nakamura (2004), Evolution of the Nankai Trough décollement from the trench into the seismogenic zone: Inferences from three-dimensional seismic reflection imaging, *Geology*, *32*(4), 273–276.

Bangs, N. L., K. D. McIntosh, E. A. Silver, J. W. Kluesner, and C. R. Ranero (2015), Fluid accumulation along the Costa Rica subduction thrust and development of the seismogenic zone, *J. Geophys. Res. Solid Earth*, *120*, 67–86, doi:10.1002/2014JB011265.

Behrmann, J. H. (1991), Conditions for hydrofracture and the fluid permeability of accretionary wedges, *Earth Planet. Sci. Lett.*, *107*(3–4), 550–558, doi:10.1016/0012-821X(91)90100-V.

Behrmann, J. H., et al. (1992), *Proceedings of Ocean Drilling Program Initial Reports*, vol. 141, Ocean Drill. Program, College Station, Tex.

Bernard, B., J. M. Brooks, and W. M. Sackett (1978), Light hydrocarbons in recent Texas continental shelf and slope sediments, *J. Geophys. Res.*, *83*, 4053–4061.

Borowski, W. S., C. K. Paull, and W. Ussler (1996), Marine pore-water sulfate profiles indicate in situ methane flux from underlying gas hydrate, *Geology*, *24*, 655–658.

Claypool, G. E., and K. A. Kvenvolden (1983), Methane and other hydrocarbon gases in marine sediment, *Annu. Rev. Earth Planet. Sci.*, *11*, 299–327.

Coffin, R., J. Pohlman, J. Gardner, R. Downer, W. Wood, L. Hamdan, S. Walker, R. Plummerg, J. Gettrus, and J. Diaz (2007), Methane hydrate exploration on the mid Chilean coast: A geochemical and geophysical survey, *J. Pet. Sci. Eng.*, *56*(1), 32–41.

Contreras-Reyes, E., E. R. Flueh, and I. Grevemeyer (2010), Tectonic control on sediment accretion and subduction off south central Chile: Implications for coseismic rupture processes of the 1960 and 2010 megathrust earthquakes, *Tectonics*, *29*, TC6018, doi:10.1029/2010TC002734.

Faber, E., and W. Stahl (1984), Geochemical surface exploration for hydrocarbons in North Sea, *AAPG Bull.*, *68*, 363–386.

Faber, E., M. Schmidt, and A. Feyzullayev (2015), Geochemical hydrocarbon exploration—Insights from stable isotope models, *Oil Gas Eur. Mag.*, *41*(2), 93–98.

Farías, M., D. Comte, S. Roecker, D. Carrizo, and M. Pardo (2011), Crustal extensional faulting triggered by the 2010 Chilean earthquake: The Pichilemu seismic sequence, *Tectonics*, *30*, TC6010, doi:10.1029/2011TC002888.

Fischer, D., J. M. Mogollón, M. Strasser, T. Pape, G. Bohrmann, N. Fekete, V. Spiess, and S. Kasten (2013), Subduction zone earthquake as potential trigger of submarine hydrocarbon seepage, *Nat. Geosci.*, *6*(8), 647–651.

Geersen, J., J. H. Behrmann, D. Völker, S. Krastel, C. R. Ranero, J. Diaz-Naveas, and W. Weinrebe (2011), Active tectonics of the South Chilean marine fore arc (35°S-40°S), *Tectonics*, *30*, TC3006, doi:10.1029/2010TC002777.

Grando, G., and K. McClay (2007), Morphotectonics domains and structural styles in the Makran accretionary prism, offshore Iran, *Sediment. Geol.*, *196*(1–4), 157–179.

Grevemeyer, I., N. Kaul, and J. L. Diaz-Naveas (2006), Geothermal evidence for fluid flow through the gas hydrate stability field off Central Chile—Transient flow related to large subduction zone earthquakes?, *Geophys. J. Int.*, *166*(1), 461–468.

Hardebeck, J. L. (2012), Coseismic and postseismic stress rotations due to great subduction zone earthquakes, *Geophys. Res. Lett.*, *39*, L21313, doi:10.1029/2012GL053438.

Heeschen, K. U., R. W. Collier, M. A. de Angelis, E. Suess, G. Rehder, P. Linke, and G. P. Klinkhammer (2005), Methane sources, distributions, and fluxes from cold vent sites at Hydrate Ridge, Cascadia Margin, *Global Biogeochem. Cycles*, *19*, GB2016, doi:10.1029/2004GB002266.

Hensen, C., M. Zabel, K. Pfeifer, T. Schwenk, S. Kasten, N. Riedinger, H. D. Schulz, and A. Boetius (2003), Control of sulfate pore-water profiles by sedimentary events and the significance of anaerobic oxidation of methane for the burial of sulfur in marine sediments, *Geochim. Cosmochim. Acta*, *67*, 2631–2647.

Hensen, C., K. Wallmann, M. Schmidt, C. R. Ranero, and E. Suess (2004), Fluid expulsion related to mud extrusion off Costa Rica—A window to the subduction slab, *Geology*, *32*(2), 201–204.

Hubbert, M. K., and W. W. Rubey (1959), Role of fluid pressure in mechanics of overthrust faulting, *Geol. Soc. Am. Bull.*, *70*, 115–166.

Husen, S., and E. Kissling (2001), Postseismic fluid flow after the large subduction earthquake of Antofagasta, Chile, *Geology*, *29*(9), 847–850.

Ikari, M. J., C. Marone, and D. Saffer (2011), On the relationship between fault strength and frictional stability, *Geology*, *39*, 83–86, doi:10.1130/G31416.1.

Jessen, G. L., S. Pantoja, M. A. Gutierrez, R. A. Quiñones, R. R. Gonzalez, J. Sellanes, M. Y. Kellermann, and K. U. Hinrichs (2011), Methane in shallow cold seeps at Mocha Island off central Chile, *Cont. Shelf Res.*, *31*, 574–581.

Keir, R., O. Schmale, M. Walter, J. Sültenfuß, R. Seifert, and M. Rhein (2008), Flux and dispersion of gases from the "Drachenschlund" hydrothermal vent at 8°18′S, 13°30′W on the Mid-Atlantic Ridge, *Earth Planet. Sci. Lett.*, *270*, 338–348.

King, G. C. P., R. S. Stein, and J. Lin (1994), Static stress changes and the triggering of earthquakes, *Bull. Seismol. Soc. Am.*, *84*(3), 935–953.

Klaucke, I., et al. (2012), Sidescan sonar imagery of widespread fossil and active cold seeps along the central Chilean continental margin, *Geo Mar. Lett.*, *32*(5–6), 489–499.

Klotz, J. et al. (1999), GPS-derived deformation of the central Andes Including the 1995 Antofagasta Mw = 8.0 earthquake, *Pure Appl. Geophys.*, *154*(3–4), 709–730, doi:10.1007/s000240050249.

Kukowski, N., and O. Oncken (2006), Subduction erosion—The "normal" mode of fore-arc material transfer along the Chilean Margin?, in *The Andes*, edited by O. Oncken et al., pp. 217–236, Springer, Berlin.

Lange, D., F. Tilmann, S. E. Barrientos, E. Contreras-Reyes, P. Methe, M. Moreno, B. Heit, H. Agurto, P. Bernard, J.-P. Vilotte, and S. Vilotte (2012), Aftershock seismicity of the 27 February 2010 Mw 8.8 Maule earthquake rupture zone, *Earth Planet. Sci. Lett.*, *317–318C*, 413–425, doi:10.1016/j.epsl.2011.11.034.

Linke, P. (2011), Scientific cruise participants 2011, in *FS SONNE Fahrtbericht/Cruise Report SO210 ChiFlux—Identification and Investigation of Fluid Flux, Mass Wasting and Sediments in the Forearc of the Central Chile Subduction Zone*, *Rep. 44*, IFM-GEOMAR, Valparaiso, Chile, doi:10.3289/IFM-GEOMAR_Rep_44_2011.

Lomnitz, C. (2004), Major earthquakes of Chile: A historical survey, 1535-1960, *Seismological Research Letters*, *75*, 368–378.
Melnick, D., and H. P. Echtler (2006), Inversion of forearc basins in south-central Chile caused by rapid glacial age trench fill, *Geology*, *34*, 709–712.
Moore, J. C., et al. (1998), Consolidation patterns during initiation and evolution of a plate-boundary decollement zone: Northern Barbados accretionary prism, *Geology*, *26*(9), 811–814.
Moreno, M., et al. (2012), Toward understanding tectonic control on the Mw 8.8 2010 Maule Chile earthquake, *Earth Planet. Sci. Lett.*, *321–322*, 152–165.
Niewöhner, C., C. Hensen, S. Kasten, M. Zabel, and H. D. Schulz (1998), Deep sulfate reduction completely mediated by anaerobic methane oxidation in sediments of the upwelling area off Namibia, *Geochim. Cosmochim. Acta*, *62*, 455–464.
Okada, Y. (1992), Internal deformation due to shear and tensile faults in a half-space, *Bull. Seismol. Soc. Am.*, *82*(2), 1018–1040.
Ranero, C. R., et al. (2008), Hydrogeological system of erosional convergent margins and its influence on tectonics and interplate seismogenesis, *Geochem. Geophys. Geosyst.*, *9*, Q03S04, doi:10.1029/2007GC001679.
Saffer, D. M., and H. J. Tobin (2011), Hydrogeology and mechanics of subduction zone forearcs: Fluid flow and pore pressure, *Annu. Rev. Earth Planet. Sci.*, *39*, 157–186.
Sahling, H., D. G. Masson, C. R. Ranero, V. Hühnerbach, W. Weinrebe, I. Klaucke, D. Bürk, W. Brückmann, and E. Suess (2008), Fluid seepage at the continental margin offshore Costa Rica and southern Nicaragua, *Geochem. Geophys. Geosyst.*, *9*, Q05S05, doi:10.1029/2008GC001978.
Schmidt, M., C. Hensen, T. Mörz, C. Müller, I. Grevemeyer, K. Wallmann, S. Mau, and N. Kaul (2005), Methane hydrate accumulation in Mound 11 mud volcano, Costa Rica forearc, *Mar. Geol.*, *216*, 77–94.
Scholz, F., C. Hensen, M. Schmidt, and J. Geersen (2013), Submarine weathering of silicate minerals and the extent of pore water freshening at active continental margins, *Geochim. Cosmochim. Acta*, *100*, 200–216.
Schumann, K., J. H. Behrmann, M. Stipp, Y. Yamamoto, Y. Kitamura, and C. Lempp (2014), Geotechnical behavior of mudstones from the Shimanto and Boso accretionary complexes, and implications for the Nankai accretionary prism, *Earth Planets Space*, *66*, 129, doi: 10.1186/1880-5981-66-129.
Screaton, E., D. Saffer, P. Henry, and S. Hunze (2002), Porosity loss within the underthrust sediments of the Nankai accretionary complex: Implications for overpressures, *Geology*, *30*(1), 19–22.
Sellanes, J., E. Quiroga, and V. A. Gallardo (2004), First direct evidences of methane seepage and associated chemosynthetic communities in the bathyal zone of Chile, *J. Mar. Biol. Assoc. U.K.*, *84*, 1065–1066.
Tebbens, S. F., and S. C. Cande (1997), Southeast Pacific tectonic evolution from early Oligocene to present, *J. Geophys. Res.*, *102*, 12,061–12,084.
Tobin, H. J., P. Vannucchi, and M. Meschede (2001), Structure, inferred mechanics, and implications for fluid transport in the décollement zone, Costa Rica convergent margin, *Geology*, *29*, 907–910.
Tsuji, T., K. Kawamura, T. Kanamatsu, T. Kasaya, K. Fujikura, Y. Ito, T. Tsuru, and M. Kinoshita (2013), Extension of continental crust by anelastic deformation during the 2011 Tohoku-oki earthquake: The role of extensional faulting in the generation of a great tsunami, *Earth Planet. Sci. Lett.*, *364*, 44–58.
Vigny, C., et al. (2011), The 2010 Mw 8.8 Maulemega-thrust earthquake of Central Chile, monitored by GPS, *Science*, *332*, 1417–1421, doi: 10.1126/science.1204132.
Völker, D., J. Geersen, E. Contreras-Reyes, and C. Reichert (2013), Sedimentary fill of the Chile Trench (32–46°S): Volumetric distribution and causal factors, *J. Geol. Soc.*, *170*, 723–736.
Zapata-Hernández, G., J. Sellanes, A. R. Thurber, L. A. Levin, F. Chazalon, and P. Linke (2014), New insights on the trophic ecology of bathyal communities from the methane seep area off Concepción, Chile (∼36°S), *Mar. Ecol.*, *35*, 1–21, doi:10.1111/maec.12051.